Nanoscale

Cite this: *Nanoscale*, 2011, **3**, 4352

www.rsc.org/nanoscale

PAPER

Enhanced cell uptake *via* non-covalent decollation of a single-walled carbon nanotube-DNA hybrid with polyethylene glycol-grafted poly(L-lysine) labeled with an Alexa-dye and its efficient uptake in a cancer cell†

Tsuyohiko Fujigaya,*[ab] Yuki Yamamoto,[a] Arihiro Kano,[c] Atsushi Maruyama[cd] and Naotoshi Nakashima*[abd]

Received 17th June 2011, Accepted 12th August 2011
DOI: 10.1039/c1nr10635j

The use of single-walled carbon nanotubes (SWNTs) for biomedical applications is a promising approach due to their unique outer optical stimuli response properties, such as a photothermal response triggered by near-IR laser irradiation. The challenging task in order to realize such applications is to render the SWNTs biocompatible. For this purpose, the stable and homogeneous functionalization of the SWNTs with a molecule carrying a biocompatible group is very important. Here, we describe the design and synthesis of a polyanionic SWNT/DNA hybrid combined with a cationic poly(L-lysine) grafted by polyethylene glycol (PLL-*g*-PEG) to provide a supramolecular SWNT assembly. A titration experiment revealed that the assembly undergoes an approximately 1 : 1 reaction of the SWNT/DNA with PLL-*g*-PEG. We also found that SWNT/DNA is coated with PLL-*g*-PEG very homogeneously that avoids the non-specific binding of proteins on the SWNT surface. The experiment using the obtained supramolecular hybrid was carried out *in vitro* and a dramatic enhancement in the cell uptake efficiency compared to that of the SWNT/DNA hybrid without PLL-*g*-PEG was found.

Introduction

Single-walled carbon nanotubes (SWNTs) have emerged as a promising tool for nanobiotechnology mainly due to their unique optical responses arising from the strong photoabsorption of near-IR (NIR) light,[1,2] which can penetrate tissue due to the transparency of the tissue in this wavelength range.[3] Photothermal generation[4] as well as the photoacoustic effect[5] induced by NIR-light irradiation and photoluminescence in the NIR region[6–10] of the SWNTs have been proposed for detecting biological events, such as ATP, H_2O_2 and NO mappings of an organism,[5–11] and for treating a tumor.[4] In addition, an efficient cell uptake originating from their sub-micron size and their unique one-dimensional shape is advantageous for such biological applications.[12] For the biological applications, stable functionalization of the SWNTs with a biocompatible group is a primary requirement because the toxicity of the SWNTs stems from the aggregation of the SWNTs in tissues as well as the binding of the SWNTs to many biological species due to the hydrophobic nature of the SWNT surfaces.[1] The SWNT functionalization based on the covalent bonding provides dispersible SWNTs;[13] whereas this approach often causes damage to the surfaces of the SWNTs, resulting in a change in the fundamental optical properties.[14,15] Furthermore, functional groups are preferentially introduced on the defect sites of the SWNTs (mostly the tip sites of the SWNTs), which produces the heterogeneous functionalization of the SWNTs.[16]

Therefore, by taking the advantages of non-destructive and homogeneous coating of the SWNTs, non-covalent functionalization through physical adsorption of molecules on the SWNT surfaces is the preferred method. Up to now, a large number of molecules including small amphiphilic or aromatic molecules and polymers have been reported to be adsorbed onto the surfaces of the SWNTs.[17,18] However, in the case of small molecules, such as surfactants, functionalization is realized by dynamic adsorption and desorption processes, in which the excess molecules in the bulk solution are indispensable to maintaining the dynamic equilibrium. Therefore, lowering the concentration of the adsorbents in the bulk solution leads to lowering the density of the functional molecules and often causes the aggregation of the SWNTs.[19] In order to improve the stability, a non-dynamic or statically stable functionalization is strongly required for the non-covalent functionalization of the SWNTs.

[a]*Department of Applied Chemistry, Graduate School of Engineering, Kyushu University, 744 Motooka, Fukuoka, Japan. E-mail: nakashima-tcm@mail.cstm.kyushu-u.ac.jp; Fax: +81-92-802-2840*
[b]*World Premier International (WPI) Research Center International Institute for Carbon-Neutral Energy Research (I2CNER), Kyushu University, 744 Motooka, Nishi-ku, Fukuoka, Japan 819-0395*
[c]*Institute for Materials Chemistry and Engineering, Kyushu University, 744-CE11 Motooka, Nishi-ku, Fukuoka, 819-0395, Japan*
[d]*Japan Science and Technology Agency (JST), Core Research of Evolutional Science & Technology (CREST), 5 Sanbancho, Chiyoda-ku, Tokyo, 102-0075, Japan*

† Electronic supplementary information (ESI) available: Additional absorption spectra, DLS plots and PL spectra. See DOI: 10.1039/c1nr10635j

Up to now, only a few systems have been reported such as stability for the non-covalent functionalization. It was reported that polyethylene glycol (PEG)-modified lipid derivatives used as the non-covalent adsorbent enabled the highly stable SWNT dispersion[20,21] and the obtained hybrids were applied for drug delivery[22] and tumor imaging *in vivo*.[5,10,23] Such a high stability *in vivo* suggests the formation of a non-dynamic hybrid between the SWNTs and lipid derivatives.

Meanwhile, we have already reported the double- and single-strand-DNA-functionalized SWNT hybrids[24–26] were stable for a long period even after the removal of the excess DNAs in the bulk solutions.[26,27] Long-term stability of a SWNT/DNA hybrid was also achieved in cells *in vitro* and allowed the stable fluorescent emission from the SWNTs due to the isolation of the hybrid for a long period.[28,29] However, a nonspecific adsorption of proteins in the solution on the SWNT/DNA has been pointed out, which might lead to a short blood circulation in the *in vivo* system.[28] Based on these backgrounds, in this study, we describe the design and fabrication of a novel SWNT/DNA hybrid that is coupled with a biocompatible PEG compound and evaluate the stability of the hybrid. As the PEGylation material for the SWNT/DNA, we chose a PEG grafted poly(L-lysine) (PLL-*g*-PEG) since the positively charged PLL main-chain is known to form a stable polyion complex with the negatively charged DNA.[30]

Experimental section

Measurements

The UV-visible-near IR absorption spectra and PL spectra were measured using a spectrophotometer (V-670, JASCO) and spectrofluorometer (SPEX Fluorolog-3, HORIBA JOBIN YVON), respectively. Nanostructure images of the hybrids were taken using an atomic force microscope (SPM-5600, Agilent Technologies, Inc.). For sample preparation, an aqueous solution of a sample was cast on mica substrates using a spin coater for 1 min at 2000 rpm and dried in a vacuum for 2 h. Both the dynamic light scattering (DLS) and ζ potential were measured using a ζ-potential and particle-size analyzer (ELSZ-2, Otsuka Electronics Co., Ltd.). Raman mappings (excitation wavelength; 785 nm) of the cells were carried out using a microscopic laser Raman spectrometer (LabRAM ARAMIS, HORIBA JOBIN YVON).

Solubilization of SWNTs using DNA

The single stranded DNA, $(dT)_{20}$, was purchased from Hokkaido System Science Co., Ltd. The purity estimated by HPLC is greater than 99%. The as-produced SWNTs (HiPco, Carbon Nanotechnologies, Inc.) were used as received. Solubilization of the SWNTs using the DNA was conducted by following reported procedures.[26] Typically, ~0.5 mg of the SWNTs was added to an aqueous solution of the DNA (5 mL, 25 μM, Tris–EDTA buffer, pH 8.0) and sonicated using a bath-type ultrasonic cleaner (Branson 5510) at a temperature below 5 °C for 1 h, followed by centrifugation (Sigma, 3K30C) at 60 000*g* and temperatures below 5 °C for 1 h. The concentration of the DNA in an aqueous solution was determined using the molar absorption coefficient of thymine, 8400 @280 nm.[31] The top 80–90% of the solution after the centrifugation was separated and filtered using a disposable syringe filter unit (DISMIC®-13CP, 0.45 μm, Advantec®).

Removal of unbound DNA from SWNT/DNA aqueous solution

In order to remove the unbound DNA, the SWNT/DNA aqueous solution was condensed using a disposable ultrafilter unit (USY-5, Advantec®) and re-suspended by the addition of Tris–EDTA buffer. The filtration was repeated seven times. A 200 μL aliquot of the SWNT/DNA aqueous solution was introduced to the HPLC system (Shimadzu) equipped with size-exclusion chromatography columns (CNT SEC-300, CNT SEC-1000 and CNT SEC-2000, 10.0 × 250 mm, Sepax Technologies, Inc.) using Tris–EDTA buffer as the eluent (flow rate; 1.0 mL min^{-1}, 25.0 °C). A 100 nM SWNT/DNA aqueous solution was prepared by diluting the obtained solution with Tris–EDTA buffer.

PEGylation of SWNT/DNA hybrid

Alexa647-modified poly(L-lysine)-*graft*-polyethylene glycol (Alexa-PLL-*g*-PEG) was synthesized as previously reported.[32] Poly(L-lysine) (PLL, 28 kDa) grafted with polyethylene glycol (PEG, 5 kDa) at a content of 37 mol% was modified by the Alexa647. A SWNT/DNA aqueous solution (100 nM, 1.7 mL) was gradually added to an Alexa-PLL-*g*-PEG aqueous solution (100 nM, 1.5 mL) with stirring at the rate of 1.0 mL h^{-1} using a micro-syringe pump (KDS200, kdScientific).

Protein adsorption to the hybrids

The SWNT/DNA and SWNT/DNA/Alexa-PLL-*g*-PEG dissolved in Tris–EDTA buffer were condensed using a disposable ultrafilter unit (USY-5, Advantec®) to 100 nM. 2 mL of the solution was then diluted with 2.0 mL of an albumin (Sigma-Aldrich) solution in a Tris–EDTA buffer solution (0.1 mg mL^{-1}).

Cellular incubation in SWNT/DNA/Alexa-PLL-*g*-PEG aqueous solution

Two mL of Alexa-PLL-*g*-PEG in Tris–EDTA buffer (100 nM) was diluted with 2.0 mL of Dulbecco's modified Eagle Medium (D-MEM, Wako Pure Chemical Industries, Ltd.) containing fetal bovine serum (FBS) and an antibiotic (GIBCO®). The SWNT/DNA/Alexa-PLL-*g*-PEG in the cell culture was added to a dish at a final SWNT condensation of about 0.04 mg mL^{-1} (27.0 nM), and the dish was incubated at 37.0 °C in a 5% CO_2 atmosphere. After incubation, the cell medium was separated from the dish, and the cells were washed using Dulbecco's Phosphate-Buffered Saline (DPBS, GIBCO®), followed by immobilization using 4% *p*-formaldehyde phosphate buffer.

Results and discussion

Preparation of DNA/SWNT hybrids

SWNTs wrapped with DNA (denoted SWNT/DNA) are prepared according to our previous paper.[26] As DNA, the oligo DNA, $(dT)_{20}$, was used in this study. Systematic studies showed that a single strand DNA with 20 mer provides one of the most

effective dispersions of the SWNTs.[33–35] We have also reported that the 20 mer oligo DNA provides a stable DNA/SWNT hybrid.[26] To remove the unbound DNA (free DNA) from the bulk solution, we have reported a chromatography-based separation method. The SWNT/DNA hybrid was highly stable and no bound DNA was detached from the SWNT surfaces.[27] Taking the scalability of the experiments into account, we newly developed a filter-based removal method of the unbound DNA. Fig. 1a shows the absorption spectra of an aqueous SWNT/DNA solution before and after the filtration. The characteristic absorption of the DNA at around 280 nm decreased after the filtration, while that of the SWNTs appeared in the near-IR (NIR) region led no such substantial change. Since the sharpness of the SWNT peaks in the NIR region is a good indicator for the degree of dispersion,[36] the identical shape of the peaks clearly states that an individual isolation of the SWNTs was maintained after the filtration. In addition, the spectrum, ranging from UV to NIR region, after the purification (Fig. 1a) is virtually identical to that obtained after the chromatography-based purification method as reported previously,[26] indicating that the composition ratio of SWCNT/DNA is maintained after the purification. It is important, although not easy, to understand the relation between the coverage of SWNTs with DNA and cell uptake. Such an approach is now under investigation in our laboratory and the results will be published in a subsequent paper. The purity of the SWNT/DNA after the filtration was monitored by a chromatography technique.[27,37] A peak attributable to the SWNT/DNA is detected in the range of 19–30 min and a small peak of the unbound DNA appeared at around 32 min (Fig. 1b).[27] Compared with the chromatogram of the SWNT/DNA before the filtration (the dotted line in Fig. 1b), we calculated that ~99.9% of the unbound DNA was removed after the filtration, and based on the chromatogram, the purity of the SWNT/DNA was estimated to be ~95%. The presented successful purification method allows us to prepare a large quantity of a high purity SWNT/DNA hybrid.

It has not been clarified how many DNA molecules are adsorbed and associated with the SWNT solubilization. We then evaluated the molar ratio between the SWNT and the DNA in the hybrid based on the combination of atomic force microscopy (AFM) and absorption spectral measurements. Fig. 1c shows the AFM image of the SWNT/DNA cast on mica. The average length of the SWNT/DNA was estimated to be ~279 nm (Fig. 1d). Shinohara *et al.* reported the absorption coefficient of the SWNT dissolved in an aqueous micelle of sodium dodecyl sulfonate (SDS) at a wavelength of 280 nm per 1 nm optical path to be $(2.9 \pm 1.1) \times 10^4$ L mol^{-1} nm^{-1} cm^{-1},[38] which allows us to calculate the number of SWNTs from their absorption spectra because SDS has no adsorption at around 280 nm (see Fig. S1 of the ESI†). Thus, by estimating the number of DNA molecules based on its absorption at 280 nm (see Fig. S2 of the ESI†), we calculated the ratio of the two components to be 4.5 DNA molecules hybridized with a single SWNT molecule. Considering that the 20 mer of oligo-DNA can wrap a SWNT with a length of ~13 nm,[39] the 4.5 DNA molecules wrap a SWNT (~280 nm) of 60 nm length, leaving a large exposed area. The partial wrapping of the SWNT by the DNA agrees well with the work of Strano *et al.*[40]

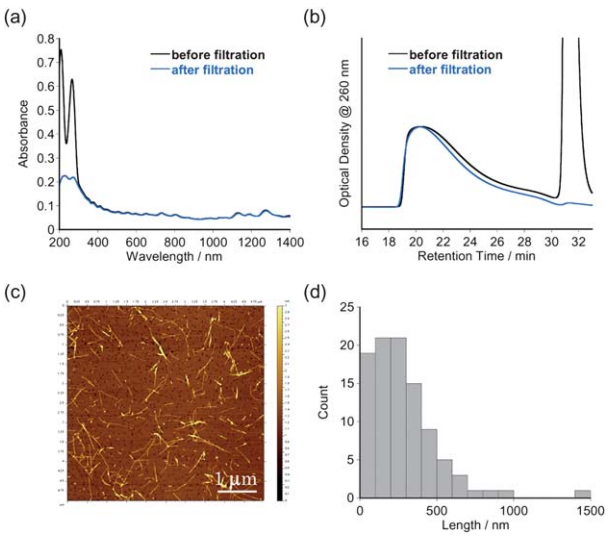

Fig. 1 (a) Absorption spectra of SWNT/DNA aqueous solution before (black line) and after (blue line) filtration. Molecular weight cut off (MWCO) value of the filter was 50 000. Cell: 1 mm. (b) Size-exclusion chromatogram of SWNT/DNA aqueous solution before (black line) and after (blue line) the filtration. (c) AFM image of SWNT/DNA after filtration on mica. (d) Length histogram of the SWNT/DNA determined from the AFM image. About 70 tubes in the image were measured.

PEGylation of SWNT/DNA hybrids with PLL-*g*-PEG

For the PEG modification (PEGylation) motif of the SWNT/DNA hybrid (Scheme 1), we chose PEG grafted poly(L-lysine) (PLL-*g*-PEG) as shown in Fig. 2a because the positively charged backbone of PLL effectively binds with the negatively charged DNAs.[41] The used PLL-*g*-PEG possesses 28 kDa of the PLL backbone and 5 kDa of the grafted PEG chain with a grafting concentration of 37 mol%. Alexa-dye was labeled to PLL-*g*-PEG (denoted Alexa-PLL-*g*-PEG) for the subsequent titration and mapping experiments. Supramolecular assembly of the SWNT/DNA with Alexa-PLL-*g*-PEG was carried out by slowly adding the SWNT/DNA solution (100 nM) in a TE buffer into 1.5 mL of the Alexa-PLL-*g*-PEG solution (100 nM) to form the PEGylated hybrid (denoted SWNT/DNA/Alexa-PLL-*g*-PEG). The dynamic light scattering (DLS) measurements from this experiment revealed that the unimodal peaks at around 200 nm appeared after the addition and such a peak was observed until an ~2.0 mL addition (0.20 nmol) of the SWNT/DNA as shown in Fig. 2b. Over the ~2.0 mL addition, the sizes of the hybrid started to increase and finally, large-sized visible aggregates were formed after the ~3.8 mL addition (0.38 nmol) (Fig. 2b; inset). We

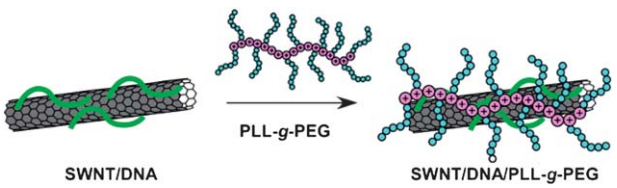

Scheme 1 Supramolecular assembly of the SWNT/DNA hybrid with PLL-*g*-PEG.

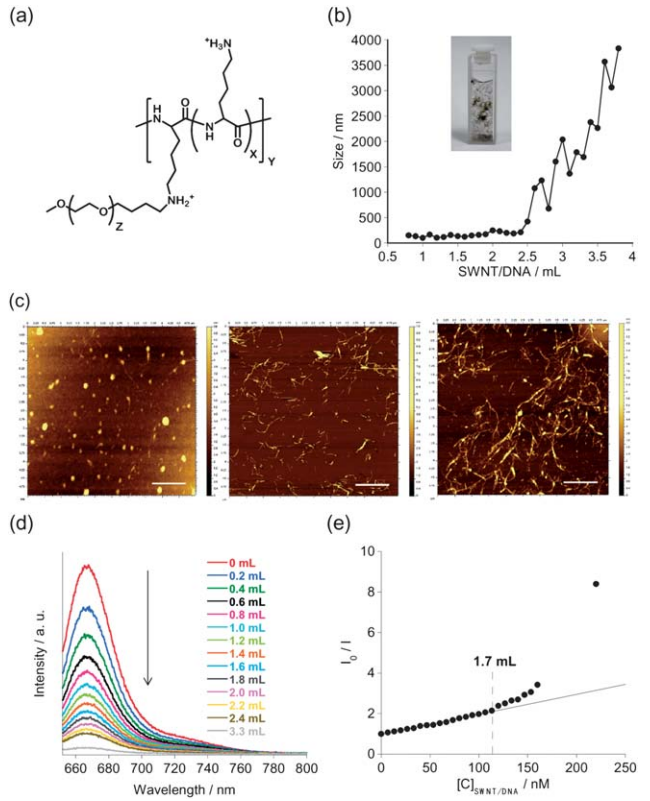

Fig. 2 (a) Chemical structure of the PLL-*g*-PEG. (b) Plot of the particle size estimated by DLS upon the addition of the DNA/SWNT to an Alexa-PLL-*g*-PEG aqueous solution (for the magnification at around the transition point, see Fig. S3 of the ESI†). (c) AFM images of the mixture of an Alexa-PLL-*g*-PEG and DNA/SWNT aqueous solution after the addition of (left) 0.7 mL, (middle) 1.7 mL, and (right) 3.2 mL of the DNA/SWNT (the sample was cast on the mica substrate, scale bar: 1 μm). (d) Change in the fluorescence spectra of an Alexa-PLL-*g*-PEG aqueous solution upon the addition of the SWNT/DNA aqueous solution. (e) Stern–Volmer plot calculated and plotted based on (c).

assumed that the Alexa-PLL-*g*-PEG was almost consumed for the assembling at the ~2.0 mL addition, and further addition of SWNT/DNA induced an aggregation due to the interaction between the negatively charged SWNT/DNA (ζ potential was −50 mV as shown in Table 1) and the positively charged SWNT/DNA/Alexa-PLL-*g*-PEG. Indeed, the ζ potential of the SWNT/DNA/Alexa-PLL-*g*-PEG at the transition point was +3 mV.

It is noted that we observed a strong photoluminescent (PL) signal of the SWNT/DNA in the NIR region until 1.7 mL addition (Fig. 3). Since SWNTs are known to emit a PL only when the SWNTs are individually isolated,[36] the presence of PL indicated the individual dissolution of the PEGylated hybrid in the solution. In contrast, no PL signal was observed after the formation of the aggregates (data not shown). The AFM

Table 1 Size of the hybrids estimated by DLS and ζ potentials of the SWNT/DNA and SWNT/DNA/Alexa-PLL-*g*-PEG aqueous solutions

	Size nm^{-1}	ζ Potential mV^{-1}
SWNT/DNA	90	−50
SWNT/DNA/Alexa-PLL-*g*-PEG	200	3

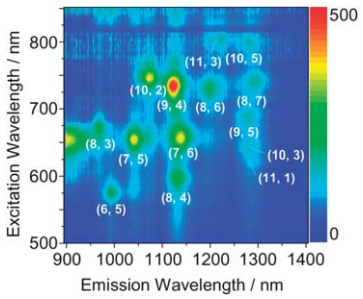

Fig. 3 (a) NIR PL mapping of the SWNT/DNA after the addition of Alexa-PLL-*g*-PEG (1.7 mL). Optical cell length: 1 cm.

measurements were carried out in order to clearly visualize the nanostructures of the obtained hybrids. Three samples were collected after the 0.7, 1.7 and 3.2 mL addition of the SWNT/DNA, and their AFM images are shown in Fig. 2c, in which a large amount of round particles or aggregated fibrous structures is observed in the samples prepared by the 0.7 and 3.2 mL addition of the SWNT/DNA, respectively. On the other hand, only isolated needle-like structures were observed after the 1.7 mL addition. We assumed that the Alexa-PLL-*g*-PEG attached along with a one-dimensional SWNT/DNA, although the free Alexa-PLL-*g*-PEG tends to form large particle structures on a mica substrate, and the formation of the large aggregated fibrous structures after the 3.2 mL addition agreed with the DLS result.

Fig. 2d shows the monitoring of the fluorescence spectra (647 nm excitation) of the Alexa-PLL-*g*-PEG upon the addition of the SWNT/DNA. Clear fluorescent quenching derived from the energy transfer from the Alexa to the SWNTs was observed, which guaranteed the close contact of the SWNT/DNA with the Alexa-PLL-*g*-PEG. The Stern–Volmer plot is displayed in Fig. 2e, where I_0, I, and $[C]_{SWNT/DNA}$ are the initial fluorescent intensity, fluorescent intensity at the concentration, and the concentration of the SWNT/DNA, respectively. It was found that the I_0/I values linearly increased at concentrations below $[C]_{SWNT/DNA} = 110$ nM by following the Stern–Volmer equation (eqn (1)), while a large deviation was observed at concentrations above $[C]_{SWNT/DNA} = 110$ nM. The result states a simple two-component assembly between the SWNT/DNA and the Alexa-PLL-*g*-PEG at concentrations below $[C]_{SWNT/DNA} = 110$ nM, while three or more components were involved in the florescent quenching at concentrations above $[C]_{SWNT/DNA} = 110$ nM. It is important to note that $[C]_{SWNT/DNA} = 110$ nM corresponds to the 1.7 mL addition of SWNT/DNA (0.17 nmol). Therefore, all the above results strongly support the presence of the transition point at ~0.17 to 0.2 nmol, in which the supramolecular PEGylation with 0.15 nmol of the Alexa-PLL-*g*-PEG was completed without leaving any excess SWNT/DNA and/or the Alexa-PLL-*g*-PEG in the bulk solution. Preparation of such a 'pure' hybrid is essential, especially for the biomedical applications to eliminate the effect from any residual 'impure' materials.

$$\frac{I_0}{I} = 1 + K_{SV} \quad (K_{SV};\ \text{Stern–Volmer constant}) \qquad (1)$$

We confirmed that the direct functionalization of the SWNTs with Alexa-PLL-*g*-PEG provided no SWNT dispersion in an

aqueous solution and found that the DNA molecules act as the glue for the PEGylation.

Dispersion of PEGylated hybrid in cultured medium

Fig. 4a and b show the comparison of the absorption spectra of the SWNT/DNA and SWNT/DNA/Alexa-PLL-*g*-PEG in water (Fig. 4a) and a D-MEM solution (Fig. 4b). Several peaks of the SWNTs were observed in the NIR region for both hybrids in water and in the D-MEM solution. The PEGylated hybrid possesses similar peak sharpness with the SWNT/DNA hybrid for both solutions, indicating the retention of the isolated state even after the supramolecular PEGylation procedure.[36] Interestingly, the peaks of the SWNT/DNA/Alexa-PLL-*g*-PEG in water slightly shifted to a longer wavelength compared to that of the SWNT/DNA, suggesting the increase in the micropolarity around the SWNTs after the PEGylation.[42–44]

We noticed that the peak positions of the SWNT/DNA/Alexa-PLL-*g*-PEG were identical both in the water and D-MEM solutions (Fig. 4a and b; indicated as the black dotted lines), whereas the peak positions of the SWNT/DNA in the D-MEM solution red-shifted by 4 nm compared to those in water. This phenomenon is explained by the adsorption of the proteins in the D-MEM solution, as pointed out by Strano *et al.*[28] As a matter of fact, the addition of albumin in an aqueous solution of the SWNT/DNA induced a similar 4 nm red-shift (Fig. 4c), while the PEGylated hybrid gave an identical spectrum even after the addition of albumin (Fig. 4d). We suppose that the SWNTs are fully coated with the PEG without leaving the accessible bare SWNT surfaces and are free from outer environmental change. Such a homogeneous coating marks a clear contrast to the covalent functionalization, in which the functionalization preferentially takes place on the defect sites and the tips of the tubes.[16] Since the sidewalls of the SWNTs are hydrophobic and easily induce a nonspecific binding site for proteins,[45] the homogeneous PEGylation is advantageous for blood circulation and tumor targeting.

It is important to note that strong PL signals were observed for the PEGylated hybrid and the signals were not quenched even after 2 weeks (see Fig. S6 of the ESI†). PL quenching is known to be caused by the oxidation of the SWNTs in solution.[25] The slight deterioration of the signal intensity is probably due to such a very slow quenching because the aggregation of the hybrids that causes the PL quenching was not observed even after 2 months.

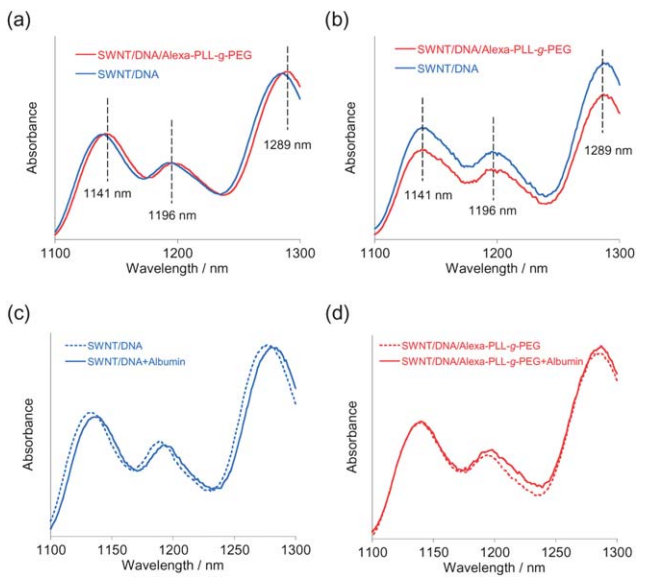

Fig. 4 Absorption spectra of the SWNT/DNA (blue line) and the SWNT/DNA/Alexa-PLL-*g*-PEG (red line) solutions in the range of 1000–1300 nm (a) in water and (b) in D-MEM solutions. Optical cell length: 1 cm. For the absorption spectra both in water and D-MEM in the range of 200–1300 nm, see Fig. S4 and S5 of the ESI†, respectively. Absorption spectra of (c) the SWNT/DNA and (d) the SWNT/DNA/Alexa-PLL-*g*-PEG in the presence (solid line) and absence (dotted line) of albumin. Optical cell length: 1 cm.

Cellular uptake of PEGylated hybrid

The PEGylated hybrid was incubated in a cell culture solution in the presence of cultured HeLa cells for 24 h. We examined the time course of cell uptake of the hybrids by Raman spectroscopy. The Raman method is a powerful technique to monitor the location of SWNTs in a high spatial resolution with long periods

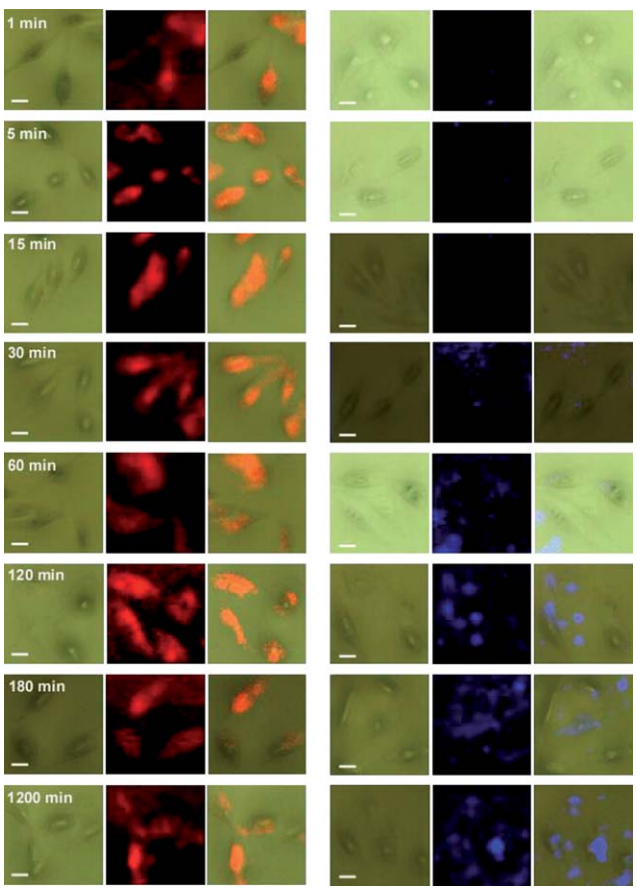

Fig. 5 Raman mappings of the cells incubated with (a) the SWNT/DNA/Alexa-PLL-*g*-PEG and (b) the SWNT/DNA for 1, 5, 15, 30, 60, 120, 180 and 1200 min (from the top to the bottom) after rinsing with a Dulbecco's PBS solution, followed by immobilization using a 4% *p*-formaldehyde phosphate buffer. Mapping was imaged by the G-band peak of the SWNTs at 1600 cm^{-1}. Scale bars: 20 μm. Pixel size: 60 × 60. Exposure time: 0.5 s at each point. Excitation wavelength: 785 nm.

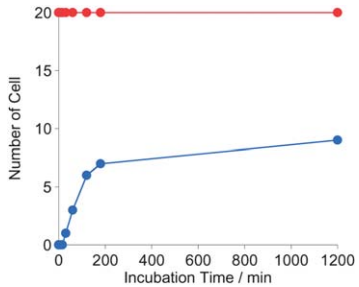

Fig. 6 Plots of the number of the cells having Raman G-band signals at a 785 nm excitation for the SWNT/DNA (blue) and the SWNT/DNA/Alexa-PLL-*g*-PEG (red) as a function of the incubation time.

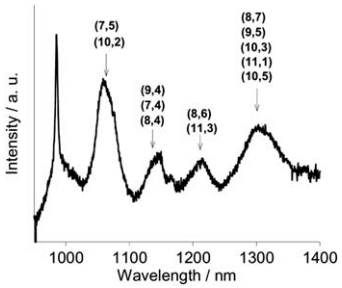

Fig. 8 PL spectrum of the SWNT/DNA/Alexa-PLL-*g*-PEG from the single cell. The measurement was carried out using an InGaAs detector. Possible SWNTs chiral indexes are assigned. Excitation wavelength: 785 nm. Exposure time: 10 s. Accumulation: 10 times.

of time since SWNTs possess an intense Raman signal as well as a minimum bleaching effect, which is the advantage of this technique in comparison to other methods such as confocal fluorescence microscopy. Raman mapping was carried out at the excitation wavelength of 785 nm for the cells having different incubation times. In Fig. 5, the optical microscope images, G-band (1600 cm^{-1}) mapping images, and their merged images are shown in the left, center and right columns, respectively.

Interestingly, strong Raman signals were observed for all the cells with the SWNT/DNA/Alexa-PLL-*g*-PEG even after 1 min incubation. In sharp contrast, a Raman signal was hardly observed for the SWNT/DNA after a 1 min incubation although after a 1200 min incubation, the Raman signal from ~40% of the cells was observed (Fig. 6). We attributed such a fast and efficient cell uptake observed for the SWNT/DNA/Alexa-PLL-*g*-PEG to the electrostatic interaction of the positively charged PLL with the negatively charged cell membrane.[46]

In the *Z*-scans of the Raman mapping, an intense Raman signal was preferentially observed on the top region of the cells compared to those from the bottom region after 5 min (Fig. 7a) and a strong signal from the bottom region was observed at 1200 min (Fig. 7b). These results clearly indicated that the PEGylated hybrid was initially attached to the surfaces of the cell surfaces and enhanced the efficiency of the uptake.

It is important to mention that not only Raman signals but the PL signals of the SWNTs were also observed from the single cell, as shown in Fig. 8, which strongly suggested that several

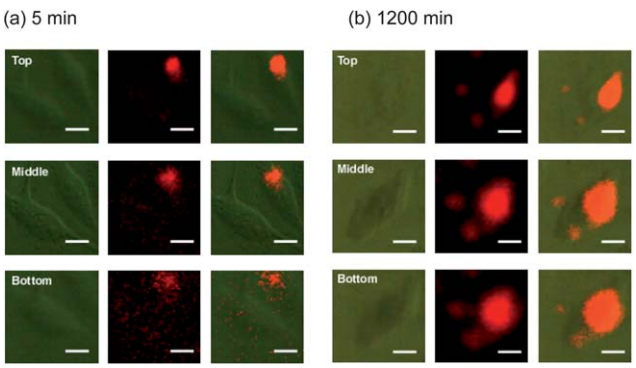

Fig. 7 Raman mappings at three different *Z*-positions of the cells incubated with the SWNT/DNA/Alexa-PLL-*g*-PEG for (a) 5 and (b) 1200 min. Scale bars: 10 μm. Pixel size: 50 × 50. Exposure time: 0.5 s at each point. Excitation: 785 nm.

PEGylated hybrids exist in an isolated state and also indicated the high stability of the hybrid as well. Such a highly stable PEGylated SWNT would be useful as a promising material for *in vivo* applications. It is expected that optimizing the sequence and length of DNA will increase the wrapping length of the SWNT surface,[47–49] yielding an increase in the density of the PEG group around SWNT after PEGylation. Investigation of toxicity of SWNTs at specific experimental conditions is very important. Since a stable SWNT wrapped by DNA is known to be effective to shield the toxicity,[50] such systematic studies using SWCNT/DNA hybrids with different coverage are required for practical applications in the *in vivo* system.

Conclusions

A highly stable SWNT/DNA (here $(dT)_{20}$) hybrid was PEGylated in a supramolecular fashion with Alexa-PLL-*g*-PEG. A titration experiment revealed that approximately one Alexa-PLL-*g*-PEG molecule was associated with the assembly of one SWNT/DNA. AFM measurements suggested that the SWNT/DNA was homogeneously enveloped with the Alexa-PLL-*g*-PEG. Such a homogeneous PEGylation effectively avoided protein adsorption onto the SWNT surfaces, while protein adsorption was recognized on the non-PEGylated SWNT/DNA. We observed a dramatic enhancement in *in vitro* cell uptake of the SWNT/DNA/Alexa-PLL-*g*-PEG hybrid compared to the hybrid without the PEGylation, indicating a significant advantage using the PEGylated SWNT/DNA hybrid. *In vivo* experiments using a cancer mouse model is currently underway in our laboratory.

Acknowledgements

This work was supported by the Global COE Program "Science for Future Molecular Systems" and Nanotechnology Network Project (Kyushu-area Nanotechnology Network) from the Ministry of Education, Culture, Sports, Science and Technology, Japan.

Notes and references

1 Z. Liu, S. Tabakman, K. Welsher and H. Dai, *Nano Res.*, 2010, **2**, 85.
2 Y. Lee and K. E. Geckeler, *Adv. Mater.*, 2010, **22**, 4076.
3 R. Weissleder, *Nat. Biotechnol.*, 2001, **19**, 316.

4 K. Nadine, S. Wong, M. O'Connell, A. Wisdom Jeffrey and H. Dai, *Proc. Natl. Acad. Sci. U. S. A.*, 2005, **102**, 11600.
5 A. D. L. Zerda, Z. Liu, S. Bodapati, R. Teed, S. Vaithilingam, B. T. Khuri-Yakub, X. Chen, H. Dai and S. S. Gambhir, *Nano Lett.*, 2010, **10**, 2168.
6 J.-H. Kim, D. A. Heller, H. Jin, P. W. Barone, C. Song, J. Zhang, L. J. Trudel, G. N. Wogan, S. R. Tannenbaum and M. S. Strano, *Nat. Chem.*, 2009, **1**, 473.
7 T. K. Leeuw, R. M. Reith, R. A. Simonette, M. E. Harden, P. Cherukuri, D. A. Tsyboulski, K. M. Beckingham and R. B. Weisman, *Nano Lett.*, 2007, **7**, 2650.
8 J.-H. Kim, J.-H. Ahn, P. W. Barone, H. Jin, J. Zhang, D. A. Heller and M. S. Strano, *Angew. Chem., Int. Ed.*, 2010, **49**, 1456.
9 H. Jin, D. A. Heller, M. Kalbacova, J.-H. Kim, J. Zhang, A. A. Boghossian, N. Maheshri and M. S. Strano, *Nat. Nanotechnol.*, 2010, **5**, 302.
10 K. Welsher, Z. Liu, S. P. Sherlock, J. T. Robinson, Z. Chen, D. Daranciang and H. Dai, *Nat. Nanotechnol.*, 2009, **4**, 773.
11 Z. Liu, S. Tabakman, S. Sherlock, X. Li, Z. Chen, K. Jiang, S. Fan and H. Dai, *Nano Res.*, 2010, **3**, 222.
12 F. E. Alemdaroglu, N. C. Alemdaroglu, P. Langguth and A. Herrmann, *Macromol. Rapid Commun.*, 2008, **29**, 326.
13 M. Prato, K. Kostarelos and A. Bianco, *Acc. Chem. Res.*, 2008, **41**, 60.
14 S. Bose, R. A. Khare and P. Moldenaers, *Polymer*, 2010, **51**, 975.
15 I. Capek, *Adv. Colloid Interface Sci.*, 2009, **150**, 63.
16 N. Karousis, N. Tagmatarchis and D. Tasis, *Chem. Rev.*, 2010, **110**, 5366.
17 T. Fujigaya and N. Nakashima, *Polym. J.*, 2008, **40**, 577.
18 N. Nakashima and T. Fujigaya, *Chem. Lett.*, 2007, **36**, 692.
19 A. Ishibashi and N. Nakashima, *Chem.–Eur. J.*, 2006, **12**, 7595.
20 G. Prencipe, S. M. Tabakman, K. Welsher, Z. Liu, A. P. Goodwin, L. Zhang, J. Henry and H. Dai, *J. Am. Chem. Soc.*, 2009, **131**, 4783.
21 Z. Liu, C. Davis, W. Cau, L. He, X. Chen and H. Dai, *Proc. Natl. Acad. Sci. U. S. A.*, 2008, **105**, 1410.
22 Z. Liu, A. C. Fan, K. Rakhra, S. Sherlock, A. Goodwin, X. Chen, Q. Yang, D. W. Felsher and H. Dai, *Angew. Chem., Int. Ed.*, 2009, **48**, 7668.
23 Z. Liu, W. Cai, L. He, N. Nakayama, K. Chen, X. Sun, X. Chen and H. Dai, *Nat. Nanotechnol.*, 2006, **2**, 47.
24 N. Nakashima, S. Okuzono, H. Murakami, T. Nakai and K. Yoshikawa, *Chem. Lett.*, 2003, **32**, 456.
25 Y. Noguchi, T. Fujigaya, Y. Niidome and N. Nakashima, *Chem.–Eur. J.*, 2008, **14**, 5966.
26 Y. Yamamoto, T. Fujigaya, Y. Niidome and N. Nakashima, *Nanoscale*, 2010, **2**, 1767.
27 Y. Noguchi, T. Fujigaya, Y. Niidome and N. Nakashima, *Chem. Phys. Lett.*, 2008, **455**, 249.
28 H. Jin, D. A. Heller and M. S. Strano, *Nano Lett.*, 2008, **8**, 1577.
29 H. Jin, D. A. Heller, R. Sharma and M. S. Strano, *ACS Nano*, 2009, **3**, 149.
30 A. Kano, K. Moriyama, T. Yamano, I. Nakamura, N. Shimada and A. Maruyama, *J. Controlled Release*, 2011, **149**, 2.
31 http://www.hssnet.co.jp/2/2_1_1_5.html#3.
32 S. W. Choi, A. Yamayoshi, M. Hirai, T. Yamano, M. Takagi, A. Sato, A. Kano, A. Shimamoto and A. Maruyama, *Macromol. Symp.*, 2007, **249–250**, 312.
33 S. R. Vogel, M. M. Kappes, F. Hennrich and C. Richert, *Chem.–Eur. J.*, 2007, **13**, 1815.
34 M. Zheng, A. Jagota, D. Semke Ellen, A. Diner Bruce, S. McLean Robert, R. Lustig Steve, E. Richardson Raymond and G. Tassi Nancy, *Nat. Mater.*, 2003, **2**, 338.
35 M. Zheng, A. Jagota, M. S. Strano, A. P. Santos, P. Barone, S. G. Chou, B. A. Diner, M. S. Dresselhaus, R. S. McLean and G. B. Onoa, *et al.*, *Science*, 2003, **302**, 1545.
36 M. J. O'Connell, S. M. Bachilo, C. B. Huffman, V. C. Moore, M. S. Strano, E. H. Haroz, K. L. Rialon, P. J. Boul, W. H. Noon and C. Kittrell, *et al.*, *Science*, 2002, **297**, 593.
37 X. Huang, R. S. McLean and M. Zheng, *Anal. Chem.*, 2005, **77**, 6225.
38 S. Kuwahara, T. Sugai and H. Shinohara, *Phys. Chem. Chem. Phys.*, 2009, **11**, 1091.
39 J. F. Campbell, I. Tessmer, H. H. Thorp and D. A. Erie, *J. Am. Chem. Soc.*, 2008, **130**, 10648.
40 E. S. Jeng, P. W. Barone, J. D. Nelson and M. S. Strano, *Small*, 2007, **3**, 1602.
41 A. Kano, K. Moriyama, T. Yamano, I. Nakamura, N. Shimada and A. Maruyama, *J. Controlled Release*, 2011, **149**, 2.
42 V. C. Moore, M. S. Strano, E. H. Haroz, R. H. Hauge, R. E. Smalley, J. Schmidt and Y. Talmon, *Nano Lett.*, 2003, **3**, 1379.
43 E. S. Jeng, A. E. Moll, A. C. Roy, J. B. Gastala and M. S. Strano, *Nano Lett.*, 2006, **6**, 371.
44 M. S. Strano, V. C. Moore, M. K. Miller, M. J. Allen, E. H. Haroz, C. Kittrell, R. H. Hauge and R. E. Smalley, *J. Nanosci. Nanotechnol.*, 2003, **3**, 81.
45 F. Lu, L. Gu, M. J. Meziani, X. Wang, P. G. Luo, L. M. Veca, L. Cao and Y.-P. Sun, *Adv. Mater.*, 2009, **21**, 139.
46 K. Kojima and T. Yamagata, *Exp. Cell Res.*, 1971, **67**, 142.
47 A. Fernando, *et al.*, *Nanotechnology*, 2009, **20**, 395101.
48 D. Roxbury, X. Tu, M. Zheng and A. Jagota, *Langmuir*, 2011, **27**, 8282.
49 X. Tu, S. Manohar, A. Jagota and M. Zheng, *Nature*, 2009, **460**, 250.
50 K. Aschberger, H. J. Johnston, V. Stone, R. J. Aitken, S. M. Hankin, S. A. K. Peters, C. L. Tran and F. M. Christensen, *Crit. Rev. Toxicol.*, 2010, **40**, 759.

